Advances in Science and Technology Research Journal

Advances in Science and Technology Research Journal, 2026, 20(9), 356–377
https://doi.org/10.12913/22998624/222637
ISSN 2299-8624, License CC-BY 4.0

Received: 2026.03.02
Accepted: 2026.07.10
Published: 2026.08.01

Docking station for unmanned aerial vehicle for autonomous railway track inspection

Antoni Kopyt[1*], Dawid Florczak[1]

[1] Faculty of Power and Aeronautical Engineering, Warsaw University of Technology, ul. Nowowiejska 24, 00-665 Warsaw, Poland
* Corresponding author's e-mail: antoni.kopyt@pw.edu.pl

ABSTRACT

UAVforRail is a fully automated docking and charging station designed to support autonomous monitoring of railway infrastructure using unmanned aerial vehicles (UAVs). The system addresses the limitations of traditional railway inspections, which are labor-intensive, time-consuming, and expose personnel to risks near active tracks. Developed for the operational needs of PKP PLK S.A., the solution is based on a modular, scalable architecture that enables repeatable inspections with minimal human intervention. The UAVforRail ecosystem integrates a multi-sensor UAV platform, an autonomous docking station, and a cloud-based control and data processing center. The primary focus of this work is the design, modeling, and validation of the docking station as a key element enabling long-term autonomous UAV operation. The station automates landing, positioning, charging, environmental protection, and data transfer. A vision-based landing subsystem using fiducial markers enables precise, repeatable docking operations. Mechanical components were developed and verified using CAD/CAE methodologies, FEM structural analysis, CFD simulations, and energy optimization studies. The UAV platform integrates RGB, LiDAR, and thermal sensors for multimodal inspection and defect detection. The system was validated through laboratory and field experiments, confirming reliable docking, charging, and operation under varying environmental conditions. The results demonstrate the feasibility of autonomous and persistent railway infrastructure monitoring using integrated UAV docking technologies.

Keywords: autonomous docking station; UAV, railway infrastructure monitoring, system integration,

INTRODUCTION

The rapid development of autonomous unmanned aerial vehicles (UAVs) has significantly expanded their role in industrial monitoring, inspection, and surveillance applications. Small multirotor platforms, particularly quadcopters, have become attractive tools for tasks such as environmental monitoring, precision agriculture, disaster response, border surveillance, infrastructure inspection, and aerial imaging, thanks to their flexibility, maneuverability, and relatively low deployment costs. In recent years, research attention has shifted from single-mission UAV deployments to long-term autonomous operation, in which drones perform repetitive tasks without direct human supervision. Achieving such autonomy, however, remains challenging, primarily due to limitations associated with onboard energy storage systems [1].

Most small UAVs rely on lithium-polymer batteries, which offer high power density but have limited capacity to meet propulsion requirements. As a result, typical flight endurance rarely exceeds 40–60 minutes, constraining mission duration and limiting the feasibility of persistent monitoring applications. This restriction becomes particularly problematic in remote or large-scale environments, where frequent manual intervention is impractical or economically inefficient. Multiple approaches have been proposed to address this limitation. Increasing onboard battery capacity can extend flight time but simultaneously increases vehicle mass, reduces payload capability, and negatively impacts aerodynamic efficiency [2]. Alternative strategies that combine energy-aware trajectory planning with optimal control have demonstrated improved efficiency, yet the resulting endurance gains are generally modest and insufficient for long-term autonomy [3]. Other concepts, including disposable or battery-dumping approaches, introduce additional logistical and safety challenges, limiting their practical adoption [4,5].

Consequently, research has increasingly focused on automated energy replenishment systems that eliminate or reduce the need for human intervention between missions. One widely investigated approach involves automatic battery replacement stations, where UAVs autonomously land and exchange depleted batteries for charged ones [6]. Battery replacement strategies are typically categorized into "cold" swapping, which requires UAV shutdown during replacement, and "hot" swapping, which maintains continuous power using a backup system [7]. Several studies have proposed and demonstrated automated swapping mechanisms, including mobile servicing stations [8], delivery-oriented battery management frameworks [9], experimental indoor hot-swapping systems [10], and prototype autonomous docking designs [11]. Despite the operational advantage of minimal downtime, frequent solution swapping can involve complex mechanical systems, increase failure risk, increase maintenance requirements, and reduce system robustness in field conditions [12].

As a result, charging-based approaches have emerged as a promising alternative. Charging strategies allow UAVs to reuse the same battery across multiple missions, simplifying system architecture while improving operational reliability. Various energy transfer methods have been explored, including wired charging, wireless inductive charging, laser-based transfer, and microwave power delivery [13–17]. Tethered UAV systems provide efficient power transfer but inherently restrict mobility and operational range. Laser and microwave energy transmission approaches remain largely experimental due to challenges related to alignment, safety, environmental sensitivity, and system complexity [18]. Solar-powered UAV concepts have also been investigated [19–22], but the available solar energy typically remains insufficient to sustain multirotor flight. Under these constraints, integrating UAVs with autonomous ground docking stations capable of charging, storage, and environmental protection has become one of the most promising approaches toward persistent UAV operation [23].

The concept of autonomous drone docking stations has therefore attracted significant research interest during the past decade [24]. Multiple review studies have systematically analyzed charging station architectures, classification methods, and operational strategies [25–28]. Existing solutions are commonly divided into stationary and mobile categories [29]. Stationary docking stations dominate current research and are typically designed as fixed or portable platforms providing automatic charging and safe storage. To achieve true long-term autonomy, these systems increasingly explore integrating renewable energy sources, particularly photovoltaics [30]. Examples include pole-mounted solar charging stations [31], photovoltaic-powered wireless charging networks [31], and conceptual solar-based docking systems [33]. Other research efforts have focused on grid-powered charging pads, wireless charging prototypes, and experimental docking mechanisms [3,34–41], as well as on novel geometries, such as inverted docking configurations that enable compact storage solutions [42–43]. Simplified docking pads and miniature charging systems targeting micro-UAV platforms have also been proposed, although many remain limited to laboratory or hobbyist scenarios [44]. Mobile docking stations constitute a complementary research direction aimed at increasing flexibility by mounting charging infrastructure on ground vehicles or autonomous rovers. Renewable-powered mobile concepts have been explored [36], alongside mobile platforms designed to support UAV swarms or delivery applications [41–43]. While mobility offers operational advantages, many systems remain conceptual or restricted to controlled environments, indicating a gap between research prototypes and robust industrial deployment. In parallel with academic progress, commercial interest in autonomous UAV docking systems has grown rapidly. A variety of industrial solutions now offer automated charging, weather-protected storage, and remote mission management capabilities [44]. Nevertheless, many market-available systems offer only basic charging pads, lacking full environmental protection or long-term storage functionality. Additionally, industrial docking stations are often tightly coupled with specific drone models, limiting interoperability and reducing flexibility for specialized applications. Only a small subset of commercial designs integrates renewable energy sources, and even fewer optimize their energy harvesting architecture for continuous autonomous operation [42–44].

While docking technologies have matured considerably, their application to large-scale industrial inspection domains introduces new challenges. Railway infrastructure represents a particularly demanding monitoring environment due to extensive track lengths, dispersed assets, and exposure to varying environmental conditions. Traditional railway inspections rely heavily on manual procedures performed by personnel working in proximity to active tracks, resulting in high operational cost, limited inspection frequency, and significant safety risks [1–4]. Increasing rail traffic density and aging infrastructure further intensify the need for more frequent, accurate diagnostics. UAV-based monitoring has therefore emerged as a transformative solution, enabling rapid data acquisition, reduced downtime, and improved safety by removing the need for human presence on tracks.

Recent advances in autonomous docking technology make the possibility of fully automated UAV inspection ecosystems tailored to railway applications a reality. Systems such as UAVforRail demonstrate the integration of autonomous docking stations with dedicated UAV platforms capable of continuous inspection workflows. These systems combine precision visual-servo landing [35–39], autonomous battery charging, secure environmental storage, and automated data transfer to cloud-based processing infrastructures, enabling high-frequency monitoring with minimal human involvement. Modular industrial-grade architectures allow scalable deployment across distributed railway networks, while AI-driven data analysis and real-time communication enhance decision-making efficiency and operational responsiveness [40–43]. Additional capabilities such as emergency power backup and support for beyond visual line of sight (BVLOS) operations further increase system reliability and reduce operational barriers [34–35].

Despite rapid technological progress in both UAV docking infrastructure and UAV-based monitoring methodologies, docking stations specifically optimized for railway inspection remain underexplored. Existing solutions are predominantly designed as general-purpose UAV servicing platforms and do not sufficiently address railway-specific constraints, such as distributed deployment along long-distance corridors, strict safety requirements, environmental exposure, and the need for continuous autonomous operation. As a consequence, the development of autonomous, scalable, and railway-oriented docking stations capable of enabling persistent UAV-based monitoring of train infrastructure constitutes an emerging research problem. Addressing this challenge requires coordinated advances in autonomous docking technologies, energy management, precision landing control, communication systems, and integration within industrial railway maintenance workflows.

In contrast to other application domains, such as pipeline inspection, forestry monitoring, or industrial asset surveillance, railway-oriented UAV docking systems must address distinct operational constraints. Railway infrastructure is inherently linear and spans long distances, requiring the deployment of multiple docking stations along extended corridors rather than within confined or localized areas. Additionally, operations are conducted in close proximity to active rail traffic, imposing strict safety, reliability, and regulatory requirements that exceed those of many other inspection scenarios. Most of the scenarios are feasible to implement, given the limited urban areas. The dock, however, has to be located at specific locations (in the future), approximately 20 [km] apart, where proper power and internet are provided. The docking station does not have to be limited regarding its parameters (size or weight). The docking station is meant to be set once in a selected location. However, the docking station must be operable under various conditions (snow, rain, and wind), and these conditions are considered in the docking requirements. The weaker element is still drone (the wind susceptibility), but the dock has also been wind-resistant.

DOCKING STATION CONCEPT FOR FORESTRY

The first concept for the docking station emerged from a research program aimed at developing one that could operate independently of an external energy source (own power source: solar panels). Its primary purpose is to support autonomous aerial surveillance of forest areas, which are often located far from existing power infrastructure. Data collected by UAVs, primarily in the form of aerial imagery, can be used for multiple applications, including assessing forest pest infestations, counting and analyzing wildlife, evaluating soil composition, estimating fertilizer and plant protection requirements, and determining crop yields. The overall architecture of the solution consists of a network of docking stations (up to ten units), each paired with a dedicated quadrotor, supported by a Proxy Server and a Remote-Control Center that enables remote supervision by a human operator.

The docking station was developed in two configurations: a stationary version and a portable version. The stationary system is permanently installed in the field and consists of a vertical pole approximately 6 meters high, anchored to a concrete foundation (Figure 1). Its architecture includes a landing platform and storage system, an automation module with a drone alignment mechanism, a control computer, a battery charging unit, communication modules, an energy harvesting subsystem optionally equipped with a solar tracker, an energy storage system, power management and distribution modules, anti-theft protection, and a data exchange module. In contrast, the portable version was designed for easier transport and rapid deployment. While it contains the same functional components, they are mounted on movable platforms to prioritize mobility. To simplify deployment, the portable configuration omits the solar tracking mechanism and instead uses fixed photovoltaic panels set at approximately 36°, which corresponds to typical operating conditions in Poland. Each docking station is designed to operate with a single UAV. The stationary version supports fully autonomous operation for several weeks, potentially providing continuous 24/7 functionality without human intervention, while the portable variant is intended for shorter deployments lasting several days. The system is designed to operate primarily between March and October, reflecting typical Polish weather conditions, and allows up to four sequential flights per day. Under these assumptions, a single station can monitor an area of approximately 400 km² within one month. Communication between the system modules is achieved using MavLink and S7/Modbus protocols, enabling reliable interaction between the UAV, docking infrastructure, and control systems.

A key component of the station is the landing platform and storage system, which primarily stores and protects the drone while it is charging. The landing platform consists of a lightweight glass-fiber composite deck supported by an aluminum frame and enclosed by a deployable protective dome. This subsystem has a total mass of approximately 58.9 kg and is designed to provide environmental protection and operational reliability. The dome is composed of two movable covers manufactured using sandwich composite technology, combining glass and carbon fibers with a foam core, resulting in a structure capable of withstanding impacts such as bird strikes with energy up to 100 [J]. When deployed, the dome provides sufficient internal space for UAV storage and enables automatic opening and closing within approximately 13 seconds. In the closed position, it provides IP55 protection against water and dust, allowing the safe operation of system components within a temperature range of 0 °C to 30 °C. Energy transfer between the docking

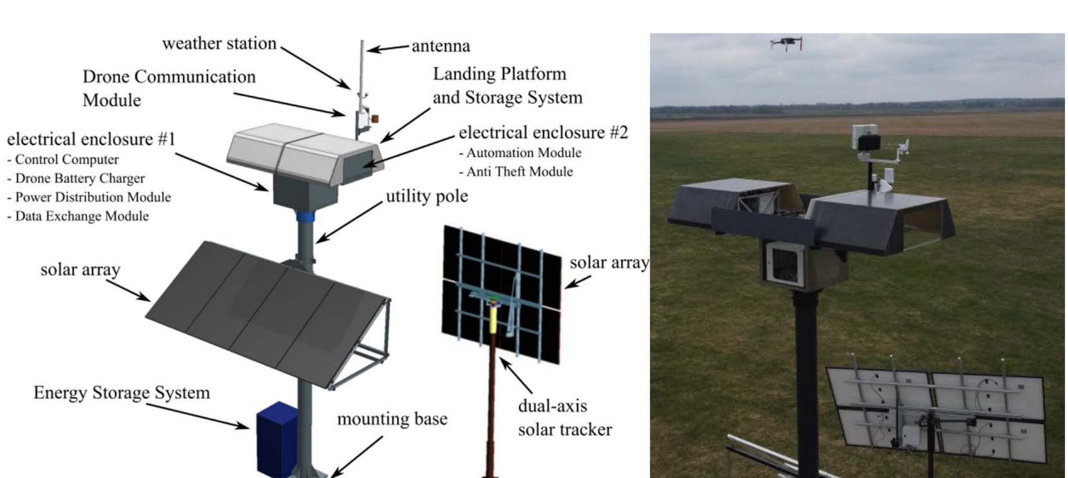

Figure 1. The concept of the docking station: (a) CAD model, (b) real system on the test field in Przasnysz [82]

station and the UAV is realized within a contact-based charging system. Four rectangular copper charging electrodes are integrated into the landing deck in a cross-shaped arrangement, matching corresponding electrodes mounted on the drone landing legs. Each electrode has a surface area of approximately 310 cm^2, enabling efficient and reliable charging after landing while maintaining mechanical simplicity and robustness suitable for long-term outdoor operation. The system was developed and implemented in the forestry sector.

The experience and research know-how allowed the WUT team to develop a second version for train inspection. The docking station was initially developed and successfully implemented for forestry monitoring applications, where it operated under real-world environmental conditions. This deployment provided valuable engineering experience covering the entire development cycle, from modeling and simulation through laboratory validation to field operation of a fully functional autonomous system. The results obtained confirmed the reliability of the docking concept and its suitability for long-term autonomous UAV operations in outdoor environments. This practical experience enabled further development of the system towards new application domains and user groups. However, transferring the solution to railway infrastructure required redefining operational requirements and system constraints. In particular, railway applications introduced stricter safety requirements, operation along linear, highly distributed infrastructure, and exposure to weather conditions. As a result, the original forestry-oriented design was not directly reused but systematically adapted and extended. Key subsystems, such as the docking interface, charging mechanism, and protective enclosure, were retained at the conceptual level but modified to meet updated operational requirements specific to railway environments. This included improvements in alignment accuracy, structural robustness, and system responsiveness to ensure reliable operation under more demanding and safety-critical conditions.

SYSTEM ARCHITECTURE AND METHODOLOGY

The UAVforRail system is structured around three core components: the UAV with a dedicated payload for monitoring (Lidar/high resolution RGB camera/Thermal camera), an autonomous charging and docking station, and a centralized control and data processing center. The architecture is designed for modularity and ease of deployment across various railway environments. The UAV is equipped with RGB, LiDAR, and thermal sensors, enabling a multimodal inspection approach that meets end users' needs. These sensors support high-resolution mapping, defect detection, and thermal anomaly identification. The UAV's onboard system includes a real-time autopilot and navigation software that can execute predefined flight plans and dynamically adapt to obstacles and changing weather conditions.

The docking station is designed to provide full autonomy in UAV operation. It includes automated mechanisms for landing, positioning, battery charging, and data offloading. The mechanical components, including opening canopies and alignment mechanisms, are modeled and verified using CAD/CAE tools such as Siemens NX and Simcenter. The system's mechanical resilience has been verified via structural, modal, and CFD simulations.

Data collected by the UAV is transferred to a cloud-based processing center. This central hub aggregates data from multiple stations and performs analysis using artificial intelligence models for object detection and defect classification. It also manages user interaction through a GUI that includes 2D/3D visualization tools, geographic annotation, and automated reporting functionalities.

The development of the UAVforRail system follows an agile, iterative research method. Given the project's complexity and innovation level, the research approach is designed to evolve in response to ongoing testing and validation feedback. Each part of the system is developed and tested in isolation before integration into the complete prototype. The engineering design of the docking station is driven by both CAD/CAE analysis and physical prototyping. The method involves simulating mechanical loads, thermal conditions, and aerodynamic behavior to improve structural integrity. Laboratory tests with sensors, such as linear displacement meters, and validation of simulation results. Simultaneously, software development for UAV control, GUI, and cloud communication is executed using simulation environments such as UAV simulators. These enable the emulation of real-world interactions without risking actual hardware during the early phases. The AI algorithms are trained using large datasets collected during test flights. The CRISP-DM method guides the development of the AI pipeline, encompassing business understanding, data understanding, modeling, and deployment. Moreover, a robust risk management framework underpins the project, addressing potential challenges such as hardware failure, regulatory delays, and integration issues. All identified risks are assigned mitigation strategies, ensuring that the project remains resilient and adaptive.

To enable precise and repeatable docking, a vision-based landing subsystem has been implemented. The system utilizes fiducial markers (e.g., ArUco-type patterns) placed on the landing platform, which are detected by the UAV's onboard RGB camera. Based on the detected marker geometry, the relative pose (position and orientation) between the UAV and the docking station is estimated in real time using a perspective-n-point (PnP) approach.

The landing process is divided into several phases. During the initial approach, the UAV navigates using GNSS RTK positioning to reach the vicinity of the docking station. Once the visual marker is detected, the control is gradually transferred to the vision-based system, which provides higher precision. The estimated pose is used in a closed-loop control scheme, where position errors in the horizontal plane (x, y), altitude (z), and yaw angle are minimized by generating appropriate control inputs to the flight controller.

In the final phase, the UAV performs a controlled descent while continuously correcting its position based on visual feedback, enabling accurate alignment with the docking interface. In case of temporary loss of visual tracking, the system can revert to GNSS-based stabilization to ensure safe operation.

Railway environments introduce additional operational challenges related to electromagnetic interference (EMI), primarily caused by overhead traction power systems and high-current infrastructure. Such conditions may affect GNSS signal quality through multipath effects and electromagnetic disturbances. To mitigate these effects, the proposed system utilizes multi-constellation GNSS with RTK corrections and integrates redundancy through vision-based localization during the final docking phase.

Communication links are designed to maintain robustness under interference conditions, with temporary data buffering and fail-safe mechanisms ensuring mission continuity. Furthermore, the reliance on short-range vision-based positioning during landing reduces sensitivity to electromagnetic disturbances.

From a broader perspective, railway diagnostics systems employ a wide range of sensing and monitoring techniques, including onboard sensors, wayside monitoring, and data-driven approaches. As shown in recent survey studies, current trends emphasize automation, continuous monitoring, and integration of multiple data sources. The UAVforRail system contributes to this domain by introducing a flexible, mobile sensing platform capable of complementing existing diagnostic infrastructure with high-resolution, on-demand inspections [45].

The UAV platform

For monitoring, data acquisition is handled by specific UAVs equipped with dedicated sensors and payloads. The most powerful and reliable system available on the market is the DJI M350 RTK. It is a professional-grade commercial UAV designed for industrial applications, featuring a maximum flight time of up to 55 minutes under ideal conditions (no payload) and a maximum takeoff weight of 9.2 kg. It measures approximately 810 × 670 × 430. mm unfolded and 430 × 420 × 430 mm folded, with an empty weight of around 6.47 kg, including batteries. The aircraft supports multiple GNSS systems (GPS, GLONASS, BeiDou, Galileo) and offers high-precision RTK positioning with horizontal and vertical accuracies of approximately ±1 cm + 1 ppm and ±1.5 cm + 1 ppm, respectively. It can withstand winds of up to 12 m/s and reach a maximum horizontal speed of 23 m/s, with a service ceiling of 5000–7000 m, depending on the props. The platform is rated IP55 for environmental protection and supports DJI enterprise gimbals, such as the Zenmuse H20/T/N, P1, and L1 series, with payload configurations (single or dual gimbals). Intelligent flight batteries (TB65) offer robust performance across a wide temperature range and can be managed with DJI's smart charging solutions.

The UAV platform can be equipped with multiple sensor types depending on the monitoring task. A typical configuration includes RGB, LiDAR, and thermal imaging sensors. The RGB imaging system (e.g., Zenmuse H20 or P1 class) provides high-resolution imagery with up to 45 MP full-frame sensors (8192 × 5460 pixels), enabling ground sampling distances (GSD) below 2 cm/pixel at typical inspection altitudes. The LiDAR unit (e.g., Zenmuse L1 class) operates with a point density of up to 240,000–480,000 points per second, supporting multiple return modes (up to 3 returns) and achieving point cloud densities exceeding 200–300 points/m² depending on flight parameters. The system provides vertical accuracy on the order of ~5 cm and horizontal accuracy of ~10 cm under RTK conditions. The thermal imaging sensor (e.g., Zenmuse H20T class) offers a resolution of 640 × 512 pixels with a thermal sensitivity (NETD) of ≤50 mK at f/1.0, enabling precise detection of temperature anomalies, with an absolute temperature measurement accuracy of approximately ±2 °C or ±2%.

DJI, despite its high quality and popularity, is not the optimal choice for conducting flights over critical infrastructure due to technical, regulatory, and security limitations. First, DJI drones are closed systems: users lack full control over the software, algorithms, and data processing, which poses significant operational and cybersecurity risks when operating near sensitive facilities. Features such as telemetry, geofencing, automatic updates, and mandatory connections to manufacturer servers can lead to unpredictable behavior, especially in situations with limited or intentionally disabled connectivity. Furthermore, political and regulatory concerns regarding the use of foreign-made drones in critical sectors have led many governments and organizations to restrict or prohibit DJI platforms in sensitive areas. Developing a custom UAV system addresses these issues by providing full control over data flow, hardware, and software tailored to mission requirements, integrating dedicated security measures, and adapting to challenging operational conditions. A proprietary platform is also more modular, scalable, and free from external limitations, making it a far superior solution for monitoring critical infrastructure. Within the project, a dedicated UAV was developed to address all the issues. The full project and simulation tests were developed. The UAV had to be the size of the M350 and have similar capabilities. Clearly, additional tests for UAV reliability were necessary, but the initial tests demonstrated that the platform meets the project's and railway monitoring requirements. The drone on the positioning platform is presented in Figure 2.

Docking station

A review of existing solutions reveals several options, but none fully enable autonomous UAV missions. Installing additional batteries provides only a slight increase in flight time, as the added mass-to-energy ratio becomes inefficient, reducing payload capacity. Another approach is to drop discharged batteries during flight, which can extend the operation by only a few minutes. Manual battery replacement by an operator is the most common method, but it cannot be applied in autonomous systems, prompting the development of docking stations for automatic battery exchange.

Battery replacement can be performed using either the "cold" or "hot" method. In the "cold" strategy, the UAV is powered off, the depleted battery is replaced, and the drone is restarted. This is problematic if the system cannot be powered remotely. In the "hot" strategy, an emergency power supply keeps the drone active during replacement. Batteries remaining in the station are recharged for reuse. Systems based on mobile or stationary docking stations have been analyzed and prototyped by [1–10]. Battery replacement saves mission time, but the mechanical complexity of such systems often lowers reliability and requires maintenance, as noted by [11–15].

An alternative for long-term autonomous operation is charging the battery without removal. Wired methods, such as tethered drones, offer high energy efficiency and virtually unlimited

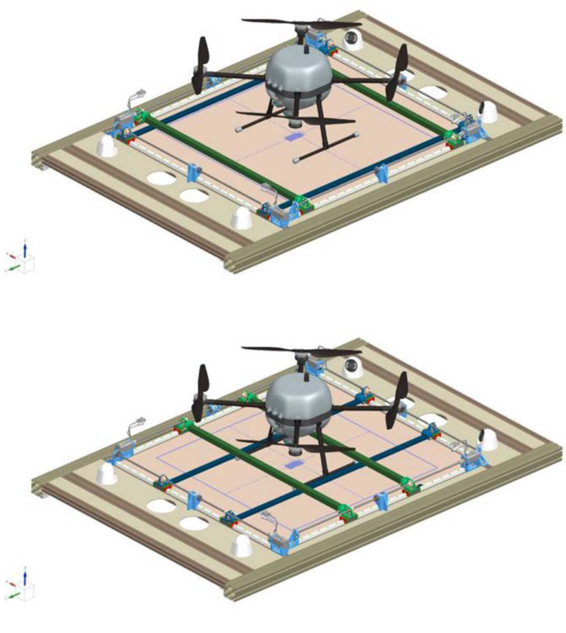

Figure 2. The dedicated UAV on the positioning platform

flight time, but limit operational range and maneuverability, and often require human supervision. Wireless charging is more promising for outdoor and autonomous missions. Solar panels on UAVs have also been explored, but the harvested energy is far less than the energy required for propulsion, making this method ineffective.

One practical solution is integrating drones with ground stations that charge batteries and provide storage. Autonomous charging stations have received significant attention recently. Detailed studies and classifications of docking stations have been presented by [16–23], highlighting trends in battery replacement and charging applications for UAVs. The solution developed by the research team aims to address the existing gaps. The final docking station project appears as shown in Figure 3.

The control center

The control center was created with a dedicated GUI for acquiring data and for viewing the drone and station cameras. Within the GUI, the operator can apply trajectories, monitor system functionality, and detect errors in functionality if they occur. The idea of the Control Center is that it can be located anywhere and is fully connected to the internet, so the operator does not have to be close to the docking station or the UAV. There is, of course, the issue of the regulations and limits set by the local FAA regarding autonomous flights. Despite this, the presented solution is intended to demonstrate the functionality and the technology in the first place. From the GUI, the operator can fully control the missions and monitor the UAV's status and all station and UAV parameters during flight. When the UAV is locked on the pad, the operator can control the data flow (sending the data from the UAV to the control station) and monitor

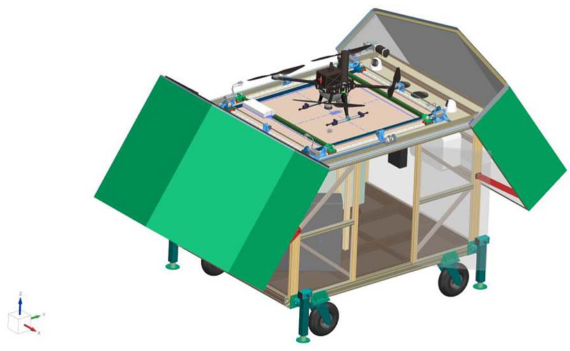

Figure 3. The project of the docking station

the battery charging process [11–13]. The overall architecture of the UAVforRail system is presented in Figure 4. The diagram illustrates the modular structure of the solution, including the UAV platform, the autonomous docking station, and the cloud-based processing center, along with the data flow and control interactions between these components. It highlights the integration of sensing, communication, energy transfer, and data processing subsystems, providing a clear representation of the system's operational workflow.

SIMULATION AND TESTS

The project encompassed comprehensive design and research activities, including the development of a conceptual system design, the design of individual subsystems, and the design, computation, and simulation work necessary before prototype components could be manufactured for laboratory testing. The main subsystems included in the study were: the station structure module, the docking platform module with lockable domes, the UAV positioning and charging system, and the automation system. Each of these was designed from scratch, leveraging the research team's existing experience. A wide range of simulations and tests were conducted:

- Energy analyses – optimization of electronic and propulsion systems, minimizing energy consumption, and ensuring the station's self-sufficiency in the event of a power outage.
- FEM simulations – analysis of the strength of the dome structure and the entire station, including the effects of wind, deflections, and cyclic loads, and optimization of design parameters.
- CFD simulations – assessment of aerodynamics during UAV takeoff and landing, determining acceptable weather conditions and landing approach directions.
- Real environment tests – tests of the docking platform movement, opening and closing of the dome, and precise positioning of the UAV, including real UAV flights.

Energy simulation and hardware optimization

The objective of the research and energy simulations was to optimize the energy use of key components of the project. For this reason,

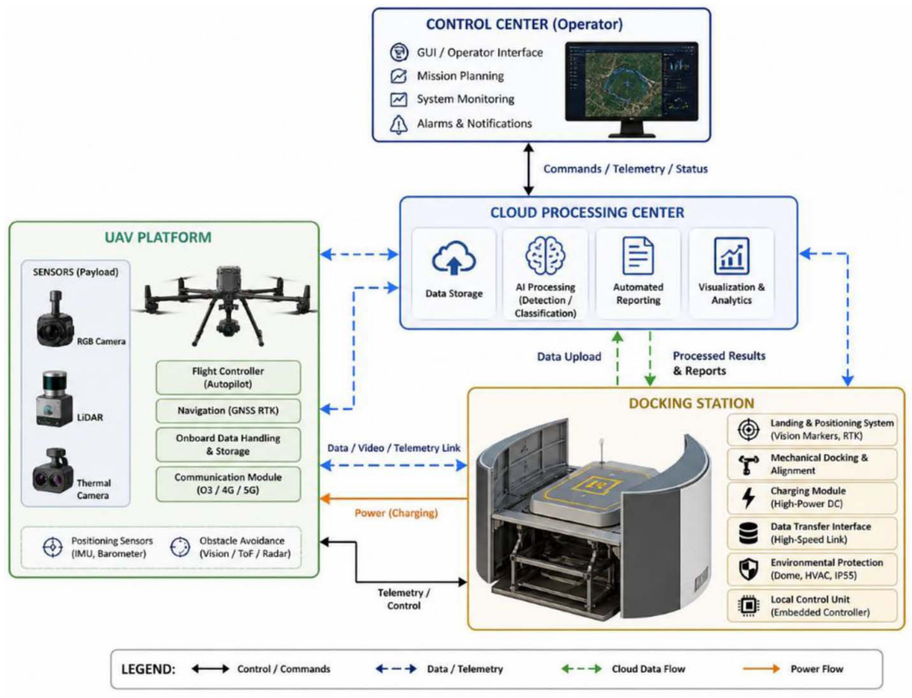

Figure 4. Architecture of the UAVforRail system

a simulation-based analysis was conducted of a solution to reduce the energy required to power the electric motors that control the drone docking station's covers. The aforementioned energy demand is related to the forces required to initiate and sustain the motion of the covers. The investigated design solution involved incorporating auxiliary springs into the opening mechanism to support the motion of the covers generated by the linear actuator. As part of the research work, a series of tasks was carried out. A physical model of the system was developed based on the CAD model. Subsequently, a mathematical model was formulated and implemented in MATLAB. A series of calculations was performed for various spring parameters. Ultimately, a specific spring model was selected, which may be installed in the actual system in the future. The analysis included simulations for different values of spring stiffness coefficients and various mounting positions [14]. The influence of the drive carriage's damping moments and travel limits was also considered. A view of the CAD model of the station frame with the cover deployment mechanism is presented in Figure 5.

Figure 6 presents a simplified schematic of the mechanism. The system is symmetrical with respect to the vertical plane perpendicular to the axis of the drive screw; therefore, for the analysis, it was sufficient to consider only half of the system (i.e., a single section).

Point A_2 (the end of the connecting rod) can move exclusively in the horizontal direction. This results from the presence of a constraint in the form of the lead screw drive carriage. The drive is self-locking, meaning that to open or close the covers, the lead screw must be driven by an electric motor (via a gearbox). Theoretically, if the screw drive were not self-locking, the mechanism could open spontaneously under the influence of gravity. Initiating motion of the system requires

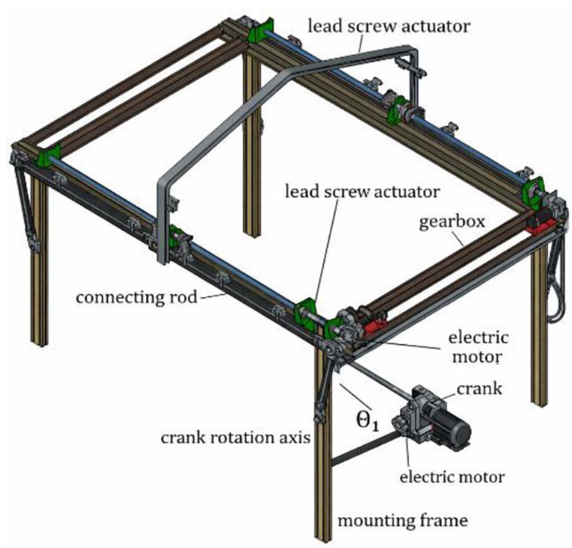

Figure 5. CAD model of the station frame with the cover deployment mechanism

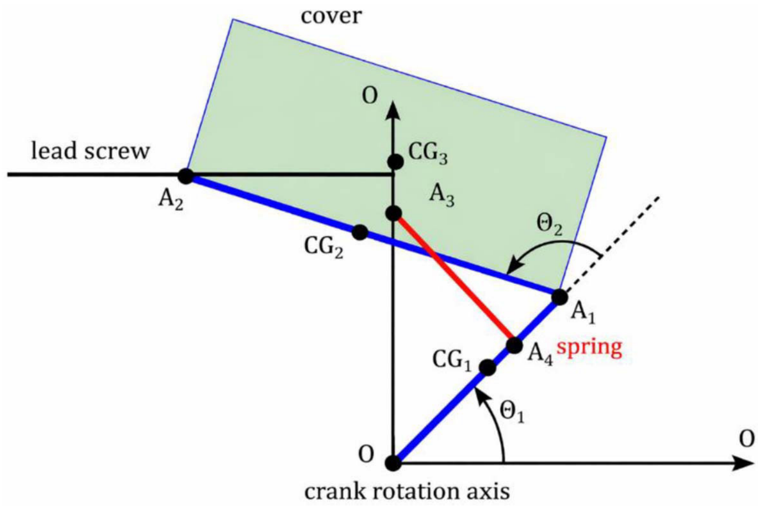

Figure 6. Simplified schematic of the system geometry adopted for the calculations

the generation of an appropriate force and, consequently, the supply of a certain amount of energy. The research described herein investigated whether it is possible to reduce this energy demand by applying springs. Various spring configurations were considered, including both torsion and linear springs. One of the key criteria was ease of installation. The introduction of springs into the system should not require significant structural modifications. Furthermore, the solution should be cost-effective and reliable. It was assumed that four linear tension springs would be installed in the system. One such spring is marked as a red element in Figure 6. One end of the spring is attached to the vertical frame column at point A_3 (a fixed point). For structural reasons, this point should be located in the upper part of the column. The other end of the spring is attached to the crank at point A_4 (a point whose position changes with the rotation of the crank). With this configuration, when the crank rotation angle Θ_1 is close to 90° (i.e., when the covers are closed), the spring should remain unstretched. Conversely, as the crank rotation angle Θ_1 approaches 0° (or even negative values), the spring is extended. Consequently, the spring force should assist the drive screw during the closing process. To visualize the results, a simple animation of the system was created. An example frame from the animation is shown in Figure 7.

It was assumed that the angular orientation of crank OA_1 is defined by the angle Θ_1 measured from the horizontal plane. The position of the crank's center of mass (point CG_1) is described by the vector:

$$r_{O-CG_1} = \begin{bmatrix} \frac{L_1}{2}\cos\Theta_1 \\ \frac{L_1}{2}\sin\Theta_1 \end{bmatrix} \tag{1}$$

where: L_1 – crank length, m, CG_1 – center of mass of the crank.

The position of the connecting rod's center of mass (point CG_2) is given by:

$$r_{O-CG_2} = \begin{bmatrix} L_1\cos\Theta_1 + \frac{L_2}{2}\cos(\Theta_1+\Theta_2) \\ L_1\sin\Theta_1 + \frac{L_2}{2}\sin(\Theta_1+\Theta_2) \end{bmatrix} \tag{2}$$

where: L_2 – connecting rod length, m, CG_2 – center of mass of the connecting rod.

The moment of inertia of the crank about its center of mass (point CG_1):

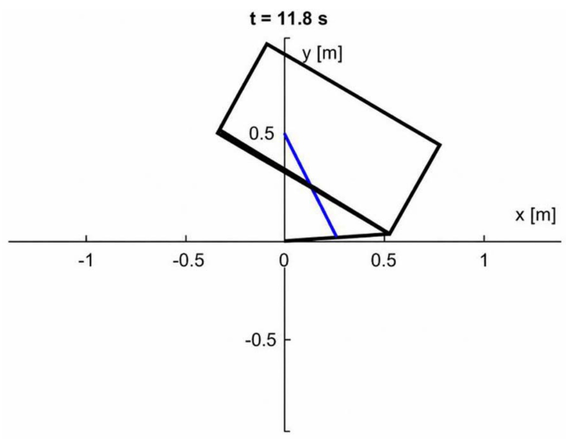

Figure 7. Example frame from the mechanism motion animation

$$I_1^{CG_1} = \frac{1}{12} m_1 L_1^2 \tag{3}$$

where: $I_1^{CG_1}$ – moment of inertia of the crank about its center of mass (point CG_1), kg·m², m_1 – mass of the crank, kg.

The moment of inertia of the connecting rod about its center of mass (point CG_2):

$$I_2^{CG_2} = \frac{1}{12} m_2 L_2^2 \tag{4}$$

where: m_2 – mass of the connecting rod, kg.

The dynamic equations of motion for the mechanism take the following form:

$$\begin{gathered} M(\mathbf{\Theta})\ddot{\mathbf{\Theta}} + C(\mathbf{\Theta}, \dot{\mathbf{\Theta}})\dot{\mathbf{\Theta}} + G(\mathbf{\Theta}) = \\ = \boldsymbol{\tau_{damp}} + \boldsymbol{\tau_{spring_1}} + \boldsymbol{\tau_{F_x}} + \\ + \boldsymbol{\tau_{spring}} + \boldsymbol{\tau_{F_{react}}} + J(\mathbf{\Theta})^T \lambda \end{gathered} \tag{5}$$

where: C – coriolis matrix, J – Jacobian.

$$\mathbf{\Theta} = \begin{bmatrix} \Theta_1 \\ \Theta_2 \end{bmatrix} \tag{6}$$

The mass matrix M has the form:

$$M = \begin{bmatrix} M_{1,1} & M_{1,2} \\ M_{2,1} & M_{2,2} \end{bmatrix} \tag{7}$$

The elements of this matrix are given as:

$$\begin{gathered} M_{1,1} = \frac{m_1 L_1^2}{4} + \\ + m_2 \left(L_1^2 + \frac{L_2^2}{4} + L_1 L_2 \cos\Theta_2 \right) + \\ + I_1^{CG_1} + I_2^{CG_2} \end{gathered} \tag{8}$$

$$\begin{gathered} M_{2,1} = M_{1,2} = \\ = m_2 \left(\frac{L_2^2}{4} + \frac{L_1 L_2}{2} \cos\Theta_2 \right) + I_2^{CG_2} \end{gathered} \tag{9}$$

$$M_{2,2} = \frac{m_2 L_2^2}{4} + I_2^{CG_2} \tag{10}$$

The matrix C is given as:

$$C(\Theta, \dot{\Theta}) = \begin{bmatrix} C_{1,1} & C_{1,2} \\ C_{2,1} & C_{2,2} \end{bmatrix} \tag{11}$$

The elements of matrix C take the form:

$$C_{1,1} = -m_2 L_1 L_2 \dot{\Theta}_2 \sin\Theta_2 \tag{12}$$

$$C_{2,1} = m_2 L_1 L_2 \dot{\Theta}_1 \sin\Theta_2 \tag{13}$$

$$C_{1,2} = -m_2 L_1 L_2 (\dot{\Theta}_1 + \dot{\Theta}_2) \sin\Theta_2 \tag{14}$$

$$C_{2,2} = 0$$

The matrix G (accounting for the effect of gravity) has the form:

$$G(\Theta) = \begin{bmatrix} G_{1,1} \\ G_{2,1} \end{bmatrix} \tag{16}$$

The elements of this matrix are defined as:

$$\begin{gathered} G_{1,1} = \left(\frac{1}{2} m_1 L_1 + m_2 L_2 \right) g \cos\Theta_1 + \\ + \frac{1}{2} m_2 L_2 g \cos(\Theta_1 + \Theta_2) \end{gathered} \tag{17}$$

$$G_{2,1} = \frac{1}{2} m_2 L_2 g \cos(\Theta_1 + \Theta_2) \tag{18}$$

Furthermore, the holonomic constraints and dynamic moments in the axes of rotation were defined:

$$\boldsymbol{\tau_{damp}} = \begin{bmatrix} -b_0 \dot{\Theta}_1 \\ -b_1 \dot{\Theta}_2 \end{bmatrix} \tag{19}$$

where: b_0, b_1 – damping coefficients (at points O and A_1 (Point at the end of the crank), respectively).

Additionally, torsional springs at the axes of rotation were implemented, enabling the possibility of mounting them. The moments generated by such springs are given as:

$$\boldsymbol{\tau_{spring}} = \begin{bmatrix} -k_0(\Theta_1 - \Theta_1^{REST}) \\ -k_1(\Theta_2 - \Theta_2^{REST}) \end{bmatrix} \tag{20}$$

where: k_0, k_1 are the stiffness coefficients of the torsional springs (at points O and A_1, respectively), Θ_1^{REST}, Θ_2^{REST} are the rest angles of the torsional springs.

Finally, the horizontal actuating force applied at the end of the connecting rod, the spring-mounted stopper model between the column and the crank, and the stopper model were also formulated and added to the system's general model. The developed mathematical model of the dome system was implemented in MATLAB R2018a as scripts. To numerically integrate the equation, it was necessary to transform it into state-space form. The state vector was defined as:

$$\boldsymbol{x} = \begin{bmatrix} \Theta_1 \\ \Theta_2 \\ \dot{\Theta}_1 \\ \dot{\Theta}_2 \end{bmatrix} \tag{21}$$

The equations of motion were integrated using the ode15 s solver. It was assumed that the time step value is 0.01 s. Additionally, it was necessary to define the initial conditions, which were as follows:

$$\boldsymbol{x}(t=0)=\begin{bmatrix}90^\circ\\90^\circ\\0\\0\end{bmatrix} \tag{22}$$

where: t – time, s.

MATLAB simulation results

It was assumed that the angular orientation of the crank OA_1 is defined by the angle Θ_1 measured from the horizontal plane. During the calculations, various values of the spring stiffness coefficient were considered. Figure 8 presents curves showing the magnitude of the force required to initiate motion of the domes (generated by the carriage to which the end of the connecting rod is attached).

The results indicate that applying a spring significantly reduces the force required to set the system in motion. Figure 9 presents the curves of the force generated by the spring. Figure 10 presents the total length of the tension spring as a function of the crank rotation angle Θ_1.

Figure 9 shows that when the covers are closed, the spring reaches its minimum length of approximately 0.2 m. Conversely, when the domes are fully deployed, the spring length is approximately 0.57 m. Figure 11 presents the work required as a function of the displacement of the carriage mounted on the drive screw. The above plot provides key evidence of energy optimization achieved. The implementation of tension springs significantly reduced the total energy required for a complete cover operation cycle. The analysis demonstrated that during the closing phase, part of the kinetic energy is converted to elastic potential energy, reducing electrical energy consumption by the drive motors. Based on the numerical simulation results, a review of spring manufacturers' offerings was conducted. Tension springs manufactured by Gutekunst were selected, specifically the RZ-153EI model. The studies undertaken and energy simulations led to the following conclusions:

- The use of tension springs in the cover mechanism effectively reduces the energy required for opening and closing operations.
- Selecting springs with an appropriate stiffness coefficient enables optimization of the overall energy balance of the system.
- Numerical simulations confirmed a reduction in the load on the electric drives without the need to modify the frame structure.
- Future work should include experimental testing of a prototype to validate the theoretical results.

CFD simulation

The objective of the conducted research was to perform an aerodynamic analysis of the station in various dome configurations (open, tilted, and closed) and at three orientations relative to the

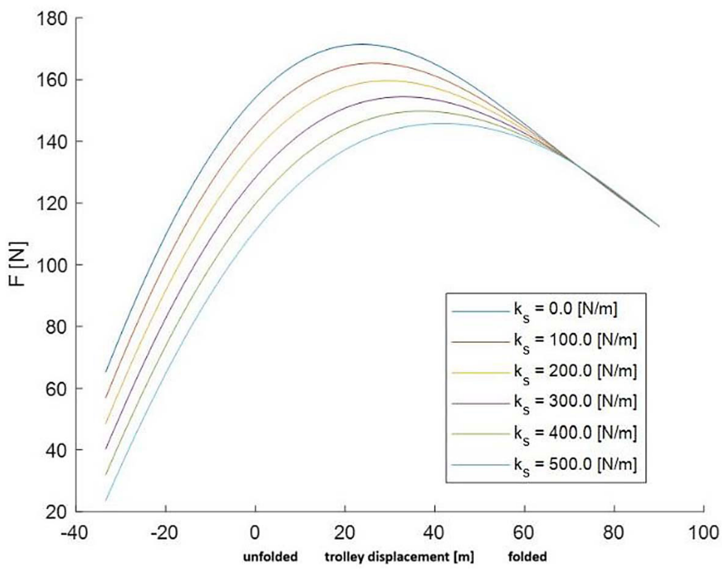

Figure 8. Force required to open/close the cover as a function of the crank rotation angle

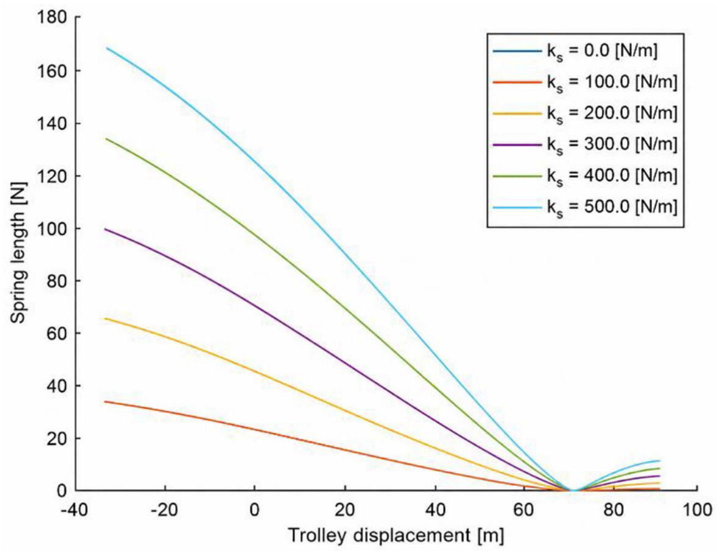

Figure 9. Tensile force in the spring as a function of the crank rotation angle

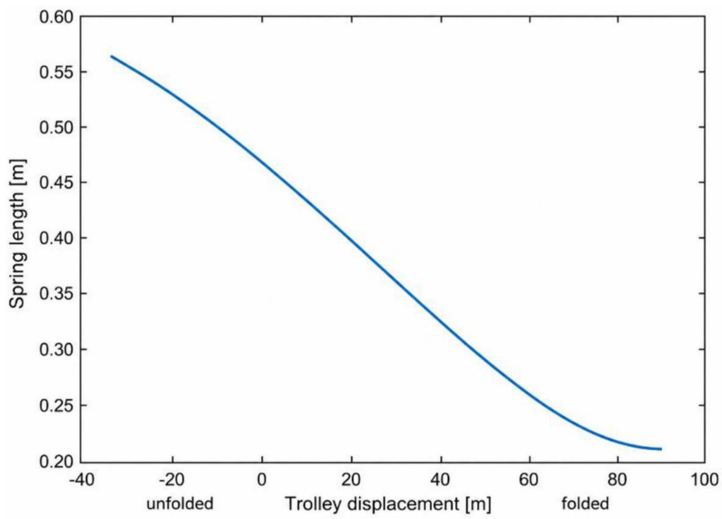

Figure 10. Total spring length as a function of the crank rotation angle

wind direction (0°, 45°, and 90°). Computational fluid dynamics (CFD) methods were used for the calculations, employing the RANS model and accounting for both typical (10 m/s) and extreme (35 m/s) wind conditions. In total, nine numerical simulations were performed to assess the aerodynamic forces acting on the station and their impact on drone operations during takeoff and landing. The first stage of the study involved preparing a simplified model of the station (Figure 12). All components that do not influence the station's aerodynamics were removed or simplified, including internal equipment, movable elements of the domes, and the shapes of the station's enclosure doors. The highest aerodynamic forces were identified for the station oriented at 45°, due to its largest projected area. Under extreme conditions, the total load reached 3250 N (Figure 13), with a significant vertical component directed upward, which could potentially lift the structure. Therefore, it is recommended to consider using guy wires or additional shields to reduce airflow under the station. The analysis also revealed the formation of an aerodynamic shadow above the landing pad, whose characteristics depend on the domes' orientation and position.

In the 45° and 90° orientations, a drone positioned on the landing pad is exposed to airflow with a velocity of approximately 40–50% of the wind speed in front of the station. In the 0° orientation, the domes shield the drone, providing more favorable operational conditions. However, in all

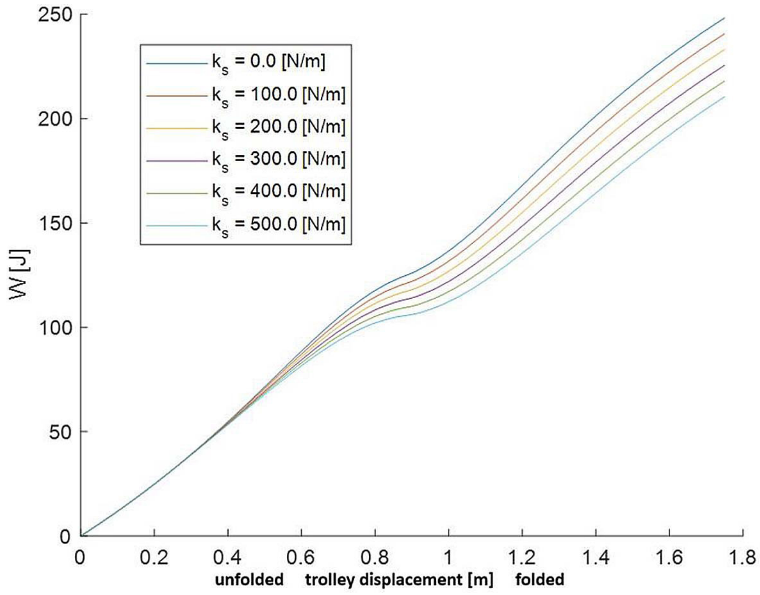

Figure 11. Total spring length as a function of the crank rotation angle

cases, strong velocity gradients are observed above the landing pad, which may complicate takeoff and landing. The results indicate that additional field studies are needed to accurately determine the station's operational limits. A view of the streamline's visualization, illustrating the effect of airflow on the open station, is shown in Figure 14.

In the next Figure 15, the velocity fields in the XY cross-section through the center of the station are shown, illustrating the flow characteristics for different configurations (open, tilted, and closed station).

Based on the analyses, it was proposed to consider alternative landing strategies, including approaches from the leeward side, to utilize the aerodynamic shadow and reduce the drone's exposure to higher wind speeds. The results provide new insights into the aerodynamic interactions between the station and the drone, form a basis for further structural analyses, and can support the development of procedures to enhance the operational safety of the system.

MES simulation and analysis

The purpose of the study was to obtain information necessary to ensure the station's strength and reliability under various wind conditions. The loads on the domes (in closed, open, and opening configurations) and on the station structure were considered. The wind conditions considered in the calculations included both operational and non-operational (extreme) scenarios. Operational conditions involved wind at 10 [m/s] (for the open configuration and during opening), while non-operational (extreme) conditions involved wind at 35 [m/s] (only for the closed structure). The wind approached the station from three directions: 0°, 45°, and 90° (Figure 1). Additionally, for the closed configuration, the domes were subjected to an additional vertical force of 5 [N], simulating accumulated leaves or a layer of snow on the station.

For the station structure, strength analyses were performed on the frame composed of interconnected aluminum profiles. Calculations were carried out for extreme conditions corresponding to a wind speed of 35 [m/s]. Wind directions considered in the analysis were 0°, 45°, and 90° (Figure 16). A modal analysis of the station was also performed to determine the natural frequencies and mode shapes of the structure. These calculations were used to identify the frequencies at which dangerous structural resonances could occur. The analysis aimed to determine whether variable dynamic loads (from wind gusts) could induce resonance when the wind frequency coincides with the structure's natural frequencies. The wind-induced loads were derived from previous CFD-based aerodynamic calculations.

The structural analysis of the domes was performed using a composite structure modeling module. For the domes, the laminated composite structure was purchased as sheets, and its exact parameters were unknown, including fiber length and orientation, the proportions of glass fibers

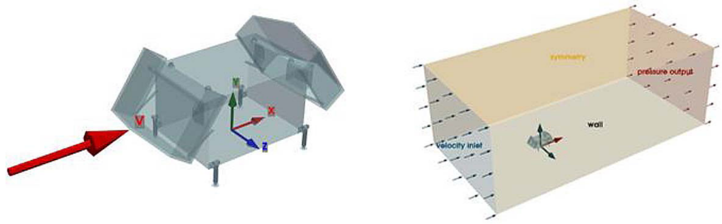

Figure 12. Simplified model of the station, together with the coordinate system (domes open), along with the schematic of the computational domain

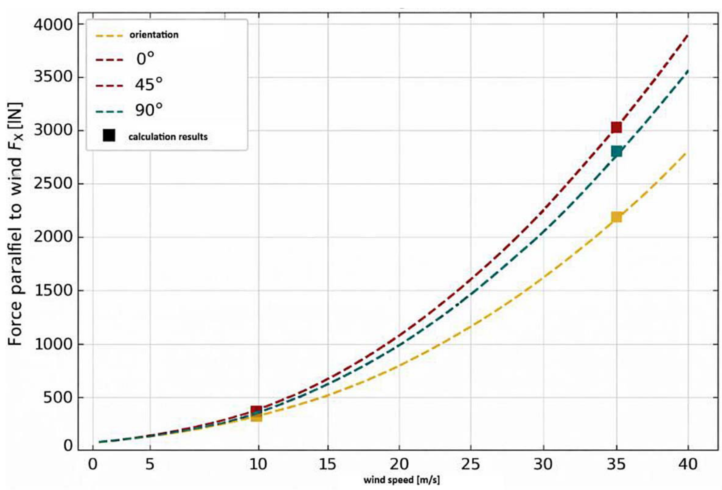

Figure 13. Estimation of the parallel component of the force for a wind speed range from 0 to 40 m/s for the configuration with closed domes

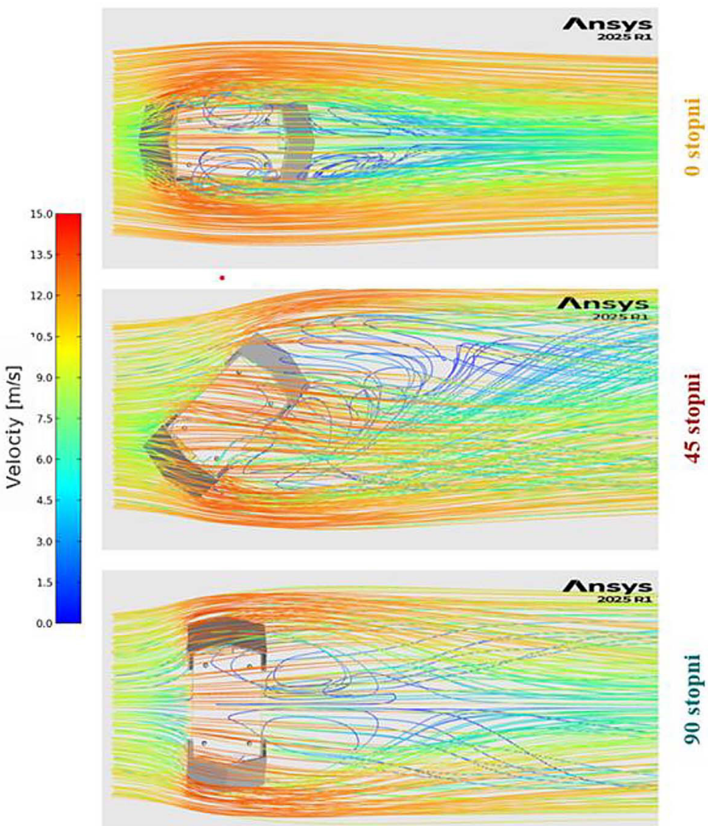

Figure 14. Simulations of the wind under three different directions

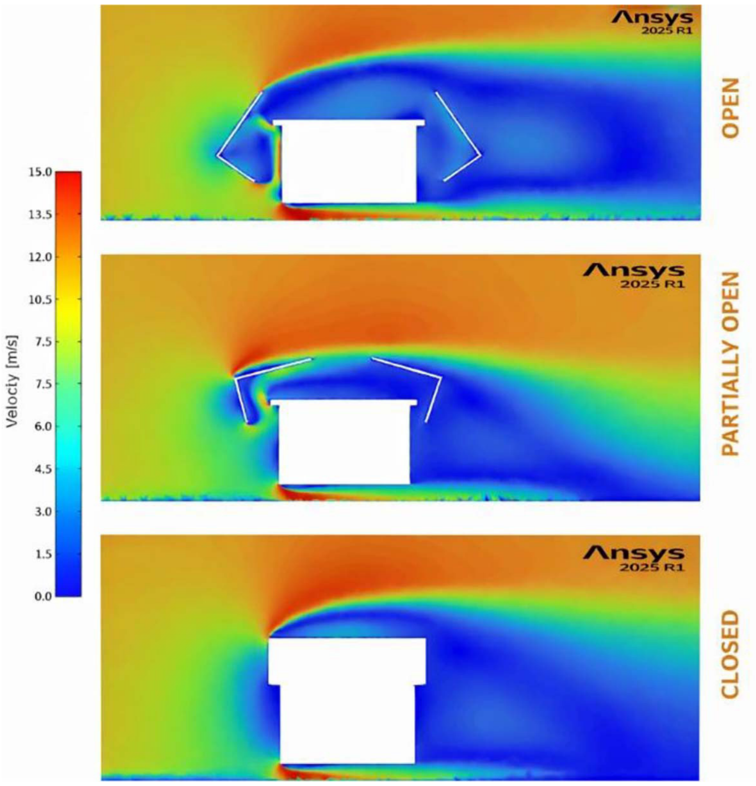

Figure 15. Dome simulation in various conditions

and polyester resin, and the physical properties of the fibers and resin. The information provided by the manufacturer was limited, including only the Young's modulus values in two directions (length and width of the composite). Based on all collected data and observations, a novel approach was adopted to model the composite despite the lack of many required parameters. The Material Designer module was used to model a composite with irregularly arranged short fibers. The proportion of glass fibers and polyester resin was selected so that the obtained Young's modulus values in both directions were close to those provided by the manufacturer. This composite model allowed the creation of a laminated structure in the module (two composite layers, 1.5 [mm] thick, separated by a 20 [mm] layer of Styrofoam) and enabled the calculations. In the analysis, pressure distributions generated during the aerodynamic calculations were used. This method is more accurate than applying a uniform aerodynamic force to the structure because it accounts for the uneven pressure distribution on the dome surfaces. The alternative method assumes an even distribution of aerodynamic force over selected surfaces. Its inaccuracy arises not only from the uniform distribution but also from the uncertainty about

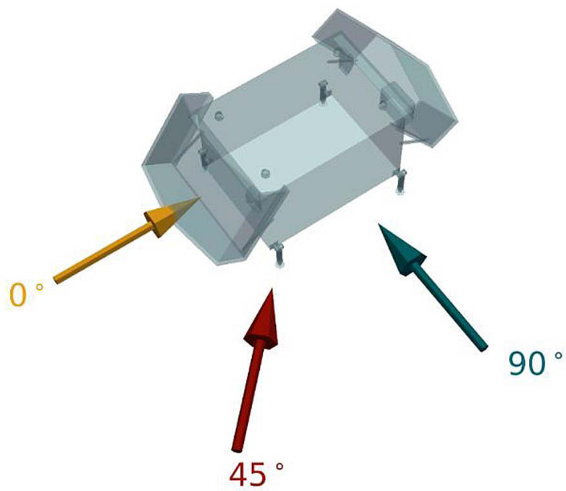

Figure 16. Investigated wind inflow directions – station orientation: 0°, 45°, 90°

which surfaces should be loaded. When the dome geometry used in the structural analysis matched that used in the aerodynamic calculations, it was possible to apply the more accurate pressure-based method. If the geometry used in the aerodynamic calculations differs from that in structural analysis (as in the station analysis, where masking panels were not included), the aerodynamic force should be recalculated. The results of the structural analysis of the domes indicate that under operational conditions (domes open or in the process of opening, loaded with wind at 10 [m/s]), regardless of the wind direction, the stresses and deformations in the composite structure are minor and do not threaten the proper functioning of the structure. For all operational cases, maximum stress does not exceed 1 [MPa], and values across most of the dome are even lower. Maximum displacements caused by these loads do not exceed 1 [mm]. Under extreme conditions, i.e., when subjected to wind at 35 [m/s] (closed domes) and including an additional vertical force pressing on the domes of 5 [N], these values increase. Nevertheless, they remain within safe limits. Maximum stresses reach several [MPa] but only affect small, localized areas. The highest stresses occur near the mounting points (8.7 [MPa] for the 0° direction) or the dome wall junctions (4.9 MPa for the 45° direction). Maximum displacements range from 8 to 9 mm, depending on the case. For wind directions of 45° and 90°, this occurs at the roof wall junctions in the transverse symmetry plane of the station. For a 0° wind direction, it appears at the midpoint of the wall's free edge, where the pressure accumulates. These values may seem relatively high; however, extreme displacements do not occur continuously. Even during short extreme gusts, displacements will oscillate between values calculated for smaller (operational) gusts and those determined for extreme conditions. The calculated maximum strains are 0.1–0.2%, as the maximum displacements are referenced to the large overall dimensions of the structure, which exceed 1 m in width and length.

In the structural analysis of the KSM station, only load-bearing elements, i.e., the frame components, were considered. The frame, consisting of aluminum profiles of various cross-sections, was modeled using one-dimensional Beam elements. The profiles are significantly longer than their cross-sectional dimensions, making the use of 1D elements appropriate and greatly accelerating the calculation process. This acceleration is essential for future work, in which the station's structure can be optimized. As previously mentioned, the station geometry used for the structural calculations differed from that used in the aerodynamic analysis (masking panels that do not bear loads were omitted). The modified geometry would result in the loss of pressure data; therefore, for the station analysis, the aerodynamic force was applied directly rather than importing the pressure distribution. Static analysis of the KSM station subjected to wind gusts of 35 m/s from three directions showed minimal structural loading. In the worst case (wind from 90°), maximum stresses slightly exceeded 13 [MPa], with bending stresses being the main component (shown in Figure 17). Axial stresses in the profiles were extremely low, reaching a maximum of approximately 1.3 MPa in tensioned profiles and 1.6 MPa in compressed profiles (for wind from 90°). The maximum displacements of the structure were also small: 1.3 mm for wind from 45° and 1.2 mm for wind from 90°. The station's profile dimensions were primarily chosen for structural safety, resulting in an over-dimensioned frame. Even under extreme wind conditions, the KSM station structure cannot be damaged. For future studies, it is advisable to consider optimizing the structure by selecting profiles with smaller cross-sections.

The final FEM analysis focused on the station's natural vibrations. It enabled the identification of critical frequencies that, if excited, could cause resonance in the structure. In this process, the vibration modes were also defined, i.e., the shape

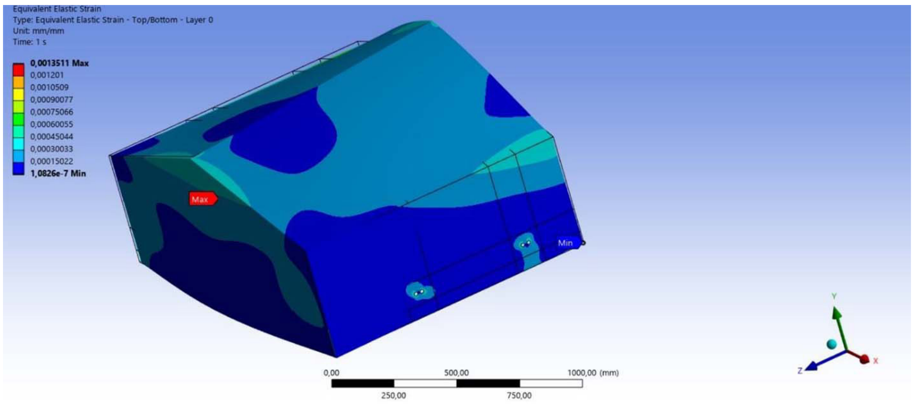

Figure 17. Deformations in the closed dome, wind inflow from 90° direction at 35 m/s velocity, vertical force 5 N

that the structure assumes when vibrating at a particular frequency. The modal analysis of the station was performed based on the previously modeled frame. Masses of station elements were included, such as the landing pad, dome module, equipment components, and walls. The masses were applied either as concentrated or distributed forces to the adjacent loaded profiles. The analysis yielded the following frequencies and vibration modes:

- Mode I: bending (motion in the transverse direction of the station, near the station legs), frequency 10.4 Hz.
- Mode II: bending-torsional (motion in the longitudinal direction of the station, near the station legs, including twisting around the station's vertical axis), frequency 15.4 Hz.
- Mode III: bending (motion in the vertical direction of the central profiles of the landing pad and station base, connected by vertical supports), frequency 16.6 Hz.

The most critical is always the first vibration mode, as it occurs at the lowest frequency. Although the frequencies obtained from the analysis are not high, it seems unlikely that wind gusts would excite vibrations at 10 Hz (as shown in Figure 18). Moreover, the study did not account for structural reinforcement elements, such as the plywood floor, the plastic masking panels for the landing pad, or additional walls. These elements were not modeled due to insufficient material data and unclear connections between the frame and the walls. It was deemed safer to omit them, as their absence lowers the frequencies of the higher vibration modes. However, the presence of these elements would increase structural stiffness, shifting all vibration frequencies upward. Including the floor and landing pad panels would be particularly significant for Mode III vibrations. It was also observed that the most vibration-prone components are the station's legs. Relative to the overall structure, which appears significantly over-dimensioned, these legs are the weakest points.

The results of the modal analysis do not raise any concerns. The structure appears to be resistant to dynamic loading from wind gusts, and varying conditions are not expected to induce resonant frequencies. The area most susceptible to bending during vibrations is the legs supporting the station. Therefore, reinforcing this area (by increasing the profile cross-section or shortening the legs) would be beneficial, shifting the frequencies toward higher values.

Real environment tests

The system's elements were previously tested under laboratory conditions, and the tests confirmed its overall functionality and capabilities. Having both – simulation and separate elements tested in laboratory conditions - the final tests could have been developed. The most important part of the research is now under development. The docking station, featuring the Control Center and a dedicated UAV, is being installed at the airport's Aviation Research Center (Figure 19). The airfield owned by the Warsaw University of Technology allows testing of various systems and hardware in a safe environment. The airspace could be closed to other aircraft, thereby eliminating the risk of collision between the systems. During the airfield tests, critical functionalities will be tested. To test the system's interoperability,

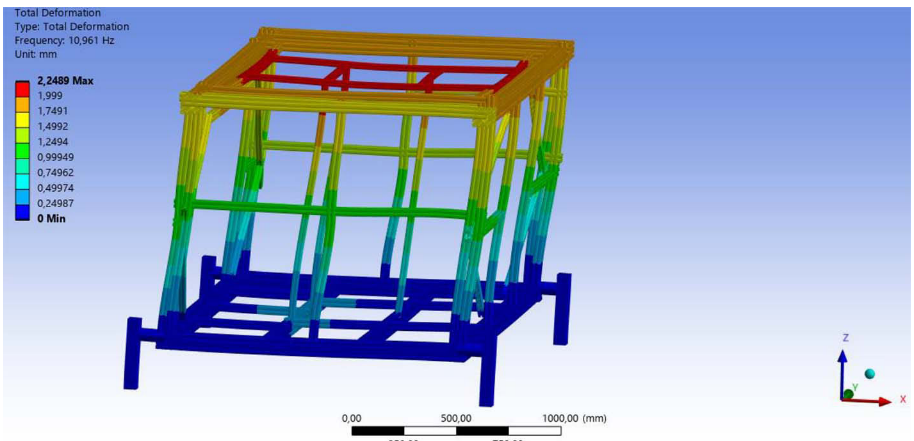

Figure 18. First vibration mode of the station structure

Figure 19. Complete docking station with the dedicated UAV

a simulated control center is used to monitor all drone activity and to evaluate the responsiveness of the GUI and backend systems. Emergency scenarios are also introduced, such as loss of GPS signal or power failure, to validate the effectiveness of backup systems and emergency protocols. These tests ensure the UAVforRail system meets both performance and safety standards before wider deployment**.**

The most critical system parameters are:

a) dome deployment time less than 120 seconds,
b) positioning mechanism operation time less than 100 seconds,
c) dedicated design for a platform with a diameter no greater than 150 cm,
d) UAV operational range of at least 4 km, with 4 km area coverage during a single mission,
e) minimum three launches per day and a power bank ensuring 3 hours of UAV operation.

The above-mentioned system requirements are being tested. Over 20 thoroughly planned missions have already been deployed successfully – battery charging, data downloading, and mission execution.

CONCLUSIONS

This study presents the design, modeling, and validation of an autonomous UAV docking station developed within the UAVforRail project, designed to enable reliable, repeatable UAV-based railway infrastructure monitoring. While UAVforRail represents a broader system integrating UAV platforms, data processing, and control infrastructure, the primary contribution of this work is the development and analysis of the docking station as a key enabler of autonomous operation. The simulations and experimental investigations conducted confirm that the proposed docking station fulfills essential functional and structural requirements. Numerical analyses, including FEM and CFD simulations, demonstrated that the structure maintains integrity and operational stability under both typical and extreme environmental conditions. The dome-based enclosure ensures environmental protection while maintaining reliable deployment and closure performance. The energy optimization study showed that the application of auxiliary tension springs significantly reduces the actuation force and total energy demand of the dome mechanism, improving the overall energy efficiency of the station. This aspect is particularly important in the context of autonomous operation within the UAVforRail system, where energy availability directly affects mission frequency and system availability. Initial laboratory and field tests confirmed the proper operation of key docking-station subsystems, including the UAV positioning interface, contact-based charging system, and automated dome mechanism. The results demonstrate that precise and repeatable UAV docking can be achieved, supporting the feasibility of long-term autonomous deployment.

Despite these promising results, several limitations must be acknowledged. The current validation has been performed under partially controlled conditions, and extended testing in real railway environments is required to fully assess system robustness. Nevertheless, the latest results showed that over 100 missions were safely completed, with the whole process (takeoff - flight – landing – charging) performed. The tests were conducted at Przasnysz airfield in controlled airspace to ensure the safety requirements. In particular, the influence of dynamic disturbances, such as airflow generated by passing trains and extreme weather conditions, was only partially investigated. Future work within the UAVforRail project will focus on long-term field validation, structural optimization to reduce system mass while maintaining safety margins, and further development of autonomous control and fault-tolerant functionalities. Additional efforts will also address integration with railway operational systems and regulatory frameworks for BVLOS missions. Overall, the developed docking station constitutes a robust and scalable component of the UAVforRail ecosystem, providing a practical foundation for continuous and autonomous railway infrastructure monitoring.

Acknowledgments

Research was conducted within the An Innovative Autonomous System for Monitoring Railway Infrastructure using Artificial Intelligence and Unmanned Aerial Vehicles (UAVforRail) project, funded by the National Research Center under the number BRIK2/0030/2022. The work is the result of multiple people involved in the project within the various parts of the research.

REFERENCES

1. Ali E, Fanni M, Mohamed AM. Design and task management of a mobile solar station for charging flying drones. E3S Web Conf; 167. Epub ahead of print 2020. https://doi.org/10.1051/e3sconf/202016705004
2. Barrett E, Reiling M, Mirhassani S, et al. Autonomous Battery Exchange of UAVs with a Mobile Ground Base. Proc. IEEE Int. Conf. Robot. Autom., 2018; 699–705.
3. Al-Obaidi MR, Hasan WZW, Mustafa MA, et al. Charging platform of chess-pad configuration for an unmanned aerial vehicle (UAV). Appl Sci 2020; 10: 1–13.
4. Lu M, Bagheri M, James AP, et al. Wireless charging techniques for UAVs: A review, reconceptualization, and extension. IEEE Access 2018; 6: 29865–29884.
5. Lee D, Zhou J, Lin WT. Autonomous Battery Swapping System for A Quadcopter. 2015 Int Conf Unmanned Aircr Syst ICUAS 2015; 118–124.
6. Lai C, Chau MT, Thai R, et al. Methods of automating power swapping mechanisms for extending UAV flight missions. Wirel Telecommun Symp 2023; 2023–April: 1–10.
7. Park S, Zhang L, Chakraborty S. Battery assignment and scheduling for drone delivery businesses. Proc Int Symp Low Power Electron Des. Epub ahead of print 2017. https://doi.org/10.1109/ISLPED.2017.8009165
8. Toksoz T, Redding J, Michini M, et al. Automated Battery Swap and Recharge to Enable Persistent UAV Missions. AIAA Infotech Aerosp Conf Exhib 2011; 0–10.
9. Saviolo A, Mao J, B RBTM, et al. AutoCharge: Autonomous Charging for Perpetual Quadrotor Missions. 2023 IEEE Int Conf Robot Autom 2023; 5400–5406.
10. Nowakowski M, Łukaszewicz A. Unmanned ground vehicle for swampy area reconnaissance with unmanned aerial vehicle support: A conceptual framework. Advances in Science and Technology Research Journal 2026; 20(1): 373–386. https://doi.org/10.12913/22998624/210510
11. Lee D, Zhou J, Lin WT. Autonomous battery swapping system for a quadcopter. ICUAS 2015.
12. Krasuski K, Bakuła M, Ciećko A, et al. Algorithms to improve unmanned aerial vehicle positioning accuracy using European Geostationary Navigation Overlay Service and System for Differential Corrections and Monitoring ionospheric corrections. Advances in Science and Technology Research Journal 2025;19(1):284–300. https://doi.org/10.12913/22998624/195195
13. Kim SJ, Lim GJ. A hybrid battery charging approach for drone-aided border surveillance scheduling. Drones 2018; 2: 1–11.
14. Al-Obaidi MR, Mustafa MA, Wan Hasan WZ, et al. Efficient Charging Pad for Unmanned Aerial Vehicle Based on Direct Contact. 2018 IEEE 5th Int Conf Smart Instrumentation, Meas Appl ICSIMA 2018 2019; 28–30.
15. Szczesiak, R., Kowalik, M., Cader, M., Pyrzanowski, P. Parametric numerical model for predicting mechanical properties of structures made

with FDM technology from polymeric materials. Polimery, 2018; 63: 9. https://doi.org/10.14314/polimery.2018.9.7

16. Fujii K, Higuchi K, Rekimoto J. Endless flyer: A continuous flying drone with automatic battery replacement. Proc - IEEE 10th Int Conf Ubiquitous Intell Comput UIC 2013 IEEE 10th Int Conf Auton Trust Comput ATC 2013, 2013; 216–223.
17. De Silva SC, Phlernjai M, Rianmora S, et al. Inverted docking station: a conceptual design for a battery-swapping platform for quadrotor UAVs. Drones 2022; 6: 1–25.
18. Lee D, Ryan T, Kim HJ. Autonomous VTOL UAV landing on a moving platform using image-based visual servoing. Proc - IEEE Int Conf Robot Autom 2012; 971–976.
19. Wang J, McKiver D, Pandit S, et al. Precision UAV Landing Control Based on Visual Detection. Proc - 3rd Int Conf Multimed Inf Process Retrieval, MIPR 2020; 205–208.
20. Xing BY, Pan F, Feng XX, et al. Autonomous landing of a micro aerial vehicle on a moving platform using a composite landmark. Int J Aerosp Eng 2019. Epub ahead of print 2019. https://doi.org/10.1155/2019/4723869
21. Nelson B, Preez J Du, Van Niekerk T, et al. Autonomous landing of a multirotor aircraft on a docking station. 2020 Int SAUPEC/RobMech/PRASA Conf SAUPEC/RobMech/PRASA 2020; 1–6.
22. Herissé B, Hamel T, Mahony R, et al. Landing a VTOL unmanned aerial vehicle on a moving platform using optical flow. IEEE Trans Robot 2012; 28: 77–89. Lai C, Chau MT, Thai R, et al. Methods of automating power swapping mechanisms. Wireless Telecomm Symp 2023.
23. Kong W, Zhang D, Wang X, et al. Autonomous landing of a UAV with a Ground-Based Actuated Infrared Stereo Vision System. IEEE Int Conf Intell Robot Syst 2013; 2963–2970.
24. Shirokova EI, Azarov AA, Wilson NG, et al. Precision Positioning of an Unmanned Aerial Vehicle for Automatic Landing. Proc 2019 IEEE Conf Russ Young Res Electr Electron Eng ElConRus 2019; 1065–1069.
25. Kim JW, Jung YD, Lee DS, et al. Landing control on a mobile platform for multi-copters using an omnidirectional image sensor. J Intell Robot Syst Theory Appl 2016; 84: 529–541.
26. Carreira TG. Quadcopter Automatic Landing on a Docking Station. University of Lisbon, 2013.
27. Tansuriyong S, Kyan M, Numata K, et al. Verification Experiment for Drone Charging. 2017 International Conference on Intelligent Informatics and Biomedical Sciences (ICIIBMS). 2017; 229–232.
28. UAV Log Viewer, https://plot.ardupilot.org/#/ (accessed 7 December 2023).
29. Commission Implementing Regulation (EU) 2019/947, https://www.easa.europa.eu/en/document-library/regulations/commission-implementing-regulation-eu-2019947
30. HEISHA, https://www.heishatech.com (accessed 9 March 2024).
31. DJI Dock, https://enterprise.dji.com/doc (accessed 6 April 2024).
32. New-R-Drone, https://www.new-r-drone.com/drone-in-a-box-avec-remplacement-de-batterie.html (accessed 9 March 2024).
33. Robert G, Antoni K, Krzysztof M, et al. Autonomous Landing Pad with a Closed Cover for a Medium-Sized Drone to Support Typical Research and Reconnaissance Tasks in the Local Environment. In: Berns K, Tokhi MO, Roennau A, et al. (eds) Walking Robots into the Real World. Cham: Springer Nature Switzerland, 2024, 164–175.
34. Głębocki R, Kopyt A. Autonomous Solar-Powered Docking Station for the Unmanned Quadrotors. In: Proceedings of the 2022 CEAS EuroGNC Conference. 2022.
35. Galimov M, Fedorenko R, Klimchik A. UAV positioning mechanisms in landing stations: Classification and engineering design review. Sensors (Switzerland) 2020; 20: 1–31.
36. Jacewicz M, Żugaj M, Głębocki R, et al. Quadrotor model for energy consumption analysis. Energies 2022; 15: 7136.
37. Głębocki R, Żugaj M, Jacewicz M. Validation of the energy consumption model for a quadrotor using Monte-Carlo simulation. Arch Mech Eng 2023; 70: 151–178.
38. Mahoor MH, Godzdanker R, Dalamagkidis K, et al. Vision-based landing of lightweight unmanned helicopters on an innovative landing platform. J Intell Robot Syst Theory Appl 2011; 61: 251–265.
39. Lee D, Ryan T, Kim HJ. Autonomous VTOL UAV landing on a moving platform using image-based visual servoing. Proc - IEEE Int Conf Robot Autom 2012; 971–976.
40. Wang J, McKiver D, Pandit S, et al. Precision UAV Landing Control Based on Visual Detection. Proc - 3rd Int Conf Multimed Inf Process Retrieval, MIPR 2020; 205–208.
41. Xing BY, Pan F, Feng XX, et al. Autonomous landing of a micro aerial vehicle on a moving platform using a composite landmark. Int J Aerosp Eng 2019. Epub ahead of print 2019. https://doi.org/10.1155/2019/4723869
42. Nelson B, Preez J Du, Van Niekerk T, et al. Autonomous landing of a multirotor aircraft on a docking station. 2020 Int SAUPEC/RobMech/PRASA Conf SAUPEC/RobMech/PRASA 2020; 1–6.Lahmeri MA, Kishk MA, Alouini MS. Charging techniques for UAV-assisted data collection: is laser power

beaming the answer? IEEE Commun Mag 2022; 60: 50–56.

43. Herissé B, Hamel T, Mahony R, et al. Landing a VTOL unmanned aerial vehicle on a moving platform using optical flow. IEEE Trans Robot 2012; 28: 77–89.
44. Kong W, Zhang D, Wang X, et al. Autonomous landing of a UAV with a ground-based actuated infrared stereo vision system. IEEE Int Conf Intell Robot Syst 2013; 2963–2970.
45. Shirokova EI, Azarov AA, Wilson NG, et al. Precision positioning of an unmanned aerial vehicle for automatic landing. Proc 2019 IEEE Conf Russ Young Res Electr Electron Eng ElConRus 2019; 1065–1069.
46. Mohsan SAH, Othman NQH, Khan MA, et al. A comprehensive review of micro UAV charging techniques. Micromachines 2022; 13: 1–30.
47. Wróbel J, Bury P, Zając M, et al. Fault detection and diagnostic methods for railway systems – a literature survey. Advances in Science and Technology Research Journal 2024; 18(6): 361–391. https://doi.org/10.12913/22998624/191762